POINT-MODELS FOR THE SET OF ORIENTED LINE-ELEMENTS – A SURVEY

MECHANISM AND MACHINE THEORY **111** 118–134 (2017) DOI: 10.1016/j.mechmachtheory.2017.01.008

Point-models for the set of oriented line-elements – a survey

Georg Nawratil

Institute of Discrete Mathematics and Geometry, Vienna University of Technology, Wiedner Hauptstrasse 8-10/104, 1040 Vienna, Austria

Abstract

We study point-models for the set $\overrightarrow{\mathcal{L}}$ of oriented line-elements by reviewing existing ones and by constructing them from different approaches proposed in the literature. We distinguish between point-models resulting from transformations and those implied by representations, where we also pursue the strategy to represent oriented line-elements by oriented line-segments with a constant length. For path planning in robotics (e.g. approximation, interpolation, optimization, ...) it is desirable to have a metric on $\overrightarrow{\mathcal{L}}$, thus we also study geometric meaningful distance measures. Based on the resulting metric spaces we finally discuss the problem of motion design.

Keywords: oriented line-element, point-model, line-segment, metric, motion design

1. Introduction and Motivation

For a large number of applications in robotics the *end-effector* has a rotational symmetry; e.g. milling, spot-welding, laser or water-jet engraving/cutting, spray-based painting, etc. For the determination of these axial symmetric tasks the rotation axis a of the tool is of importance as well as the location of the *tool tip* A, which is also known as *tool center point* (see Figure 1). In addition, the orientation of the line a has to be taken into account (see Figure 2), thus we consider the oriented line $\overrightarrow{\mathsf{a}}$.

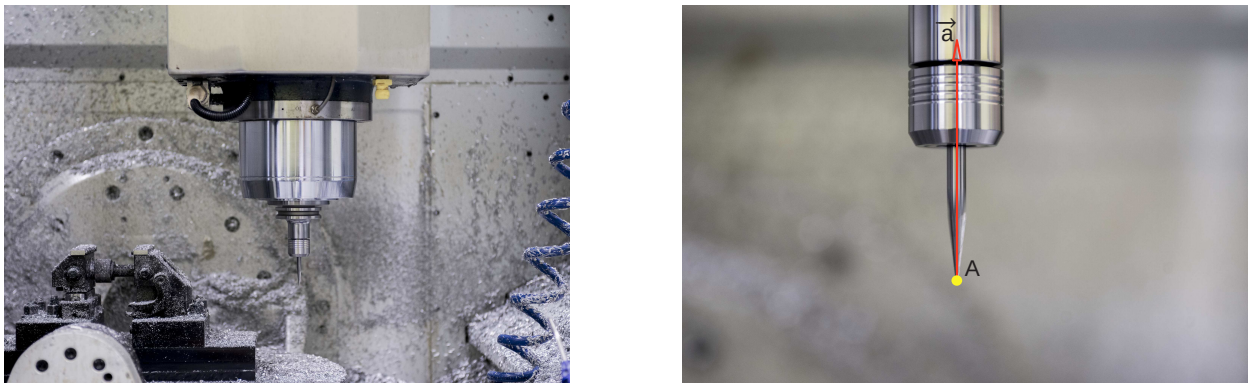

Figure 1: End-effector with rotational symmetry represented by the oriented axis $\overrightarrow{\mathsf{a}}$ and the tool tip A. Both pictures by courtesy of Florian Rist (Vienna University of Technology, Department for 3D Design and Model Making).

The two geometric objects A and $\overrightarrow{\mathsf{a}}$ can be combined to a so-called oriented line-element $(\mathsf{A}, \overrightarrow{\mathsf{a}})$, which is also known as an oriented pointed line (e.g. [1]) or point-line (e.g. [2]) in the literature. Up to the author's knowledge oriented line-elements were firstly defined by De Saussure [3] in the following way:

Definition 1. *Soit D une droite affectée d'une sens indiqué par une flèche et M un point de cette droite; la figure* (MD) *est un point dirigé.*

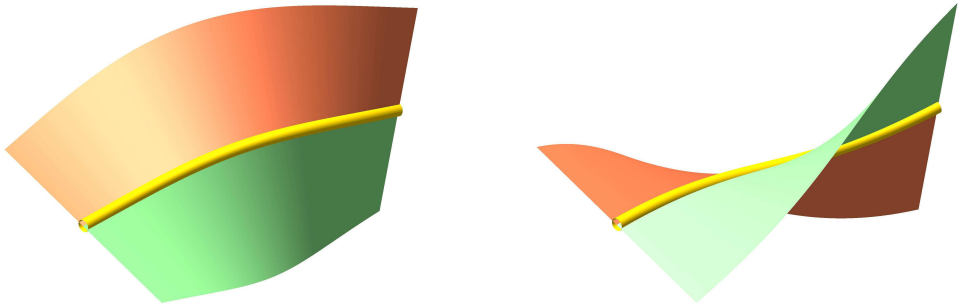

Figure 2: These figures point out the importance of the orientation of the line-element for path-planing between two given poses. The end-poses in both pictures only differ by their orientation, while the starting poses are identical.

These "directed points" can also be considered within the theory of flags, which seems to go back to De Saussure [4] as well. From this point of view an oriented line-element is an oriented partial flag of the Euclidean 3-space $\mathbb{R}^3$, which can be completed by an oriented plane $\overrightarrow{\alpha}$ with $\mathsf{a} \in \alpha$ (see also the contemporary works [1, 5, 6]). This complete flag $(\mathsf{A}, \overrightarrow{\mathsf{a}}, \overrightarrow{\alpha})$ of $\mathbb{R}^3$ can be transformed into any other complete flag $(\mathsf{B}, \overrightarrow{\mathsf{b}}, \overrightarrow{\beta})$ of $\mathbb{R}^3$ by an orientation preserving isometry (= Euclidean displacement). As a consequence the set of oriented complete flags $\overrightarrow{\mathcal{F}}$ is isomorphic to the group SE(3) of Euclidean displacements (cf. [6, Theorem 5.1]). Therefore, an oriented complete flag corresponds with a so-called *"soma"* in the notation of Study [7] and the Study quadric can be used as a point-model for $\overrightarrow{\mathcal{F}}$, which can be summed up in the following theorem (cf. [6, Theorem 5.2]):

Theorem 1. *There exists a bijection between* $\overrightarrow{\mathcal{F}}$ *and the real points* $(q_0 : q_1 : q_2 : q_3 : \widehat{q}_0 : \widehat{q}_1 : \widehat{q}_2 : \widehat{q}_3)$ *of the* 7*-dimensional projective space* $\mathbb{P}^7$ *located on the Study quadric*

$$q_0\widehat{q}_0 + q_1\widehat{q}_1 + q_2\widehat{q}_2 + q_3\widehat{q}_3 = 0, \tag{1}$$

which is sliced along the 3*-dimensional space* $q_0 = q_1 = q_2 = q_3 = 0$.

Analogously, it can be seen that the set of oriented line-elements of $\mathbb{R}^2$ is isomorphic to the group of planar Euclidean displacements. Therefore, the kinematic mapping of Blaschke [8] and Grünwald [9] implies the following point-model:

Theorem 2. *There exists a bijection between the set of oriented line-elements of* $\mathbb{R}^2$ *and the real points* $(q_0 : q_1 : \widehat{q}_2 : \widehat{q}_3)$ *of the* 3*-dimensional projective space* $\mathbb{P}^3$*, which is sliced along the line* $q_0 = q_1 = 0$.

As aforementioned, the practical application in robotics rise the question for a point-model of the set $\overrightarrow{\mathcal{L}}$ of oriented line-elements of $\mathbb{R}^3$, which can be used for motion design based on well-known methods for curves (freeform techniques, interpolation, approximation, ...). This approach is a standard technique for the design of Euclidean motions, where inter alia the point-models of Theorems 1 and 2 are used (e.g. [10, 11, 12, 13]).

1.1. Requirements of a point-model

One important property of the point-models of Theorems 1 and 2 is that a change of the fixed frame and the moving frame (which are both linear transformations in $\mathbb{R}^3$) implies a linear transformation[1] of the point-model. We also demand from our point-model $\overrightarrow{\mathcal{L}}$ to have this property as in this way linear curve design algorithms (cf. Section 4) remain invariant under the choice of the fixed and moving frame. A trivial example for a point-model, which does not fulfill this requirement is the following one, where $(A_0 : A_1 : A_2 : A_3)$ are the homogenous coordinates of A and (a_1, a_2, a_3) denotes the direction vector of $\overrightarrow{\mathsf{a}}$:

[1] In the case of Theorem 1 and 2 it is even a linear automorphism.

Theorem 3. *There is a bijection between* $\overrightarrow{\mathcal{L}}$ *and the real points* $(A_0 : A_1 : A_2 : A_3 : a_1 : a_2 : a_3)$ *of the* 6*-dimensional projective space* $\mathbb{P}^6$ *located on the quadric*

$$(A_0^2 + A_1^2 + A_2^2 + A_3^2) - (a_1^2 + a_2^2 + a_3^2) = 0, \tag{2}$$

which is sliced along the hyperplane $A_0 = 0$.

Remark 1. Alternatively, the points of the non-sliced point-model of Theorem 3 can be interpreted as the tangents to the unit-hypersphere of $\mathbb{R}^4$ (cf. [14, Sections 6 and 7]). A similar characterization of $\overrightarrow{\mathcal{L}}$ is implied by Selig's construction based on stereographic projection (cf. [15, pp. 242–243]). ◇

In total our point-model $\mathcal{P}$ should have the follow three properties:

P1 The point-model $\mathcal{P}$ is an algebraic variety.

P2 The underlying kinematic mapping $\overrightarrow{\mathcal{L}} \to \mathcal{P}$ is a bijection.

P3 A change of the moving and the fixed frame implies a linear transformation of the point-model $\mathcal{P}$.

As in our case the moving space Σ_0 degenerates into an oriented line $\overrightarrow{\mathsf{x}}_0$, the moving frame $\mathcal{F}_0(\mathsf{U}_0)$ is determined by one point on this line; namely the origin U_0. Moreover, we have to define the identity transformation; i.e. how is the moving frame $\mathcal{F}_0(\mathsf{U}_0)$ relatively located with respect to the fixed frame $\mathcal{F}(\mathsf{U}, \overrightarrow{\mathsf{x}}, \overrightarrow{\mathsf{y}}, \overrightarrow{\mathsf{z}})$, where the coordinate axes $\overrightarrow{\mathsf{x}}, \overrightarrow{\mathsf{y}}, \overrightarrow{\mathsf{z}}$ form a right-handed Cartesian system. Without loss of generality we can assume that U_0 coincides with the origin U of $\mathcal{F}$ and that $\overrightarrow{\mathsf{x}}_0$ coincides with $\overrightarrow{\mathsf{x}}$ (including orientation). The coordinates of the point $\mathsf{A} \in \Sigma_0$ with respect to the moving frame $\mathcal{F}_0$ is given by a_0.

1.2. Outline

To the best knowledge of the author there is no detailed study of point-models for the set $\overrightarrow{\mathcal{L}}$ of oriented line-elements until now. Therefore, we review existing point-models and construct point-models from different approaches proposed in the literature. We distinguish between point-models resulting from transformations (cf. Section 2) and those implied by representations (cf. Section 3), where we also pursue the strategy to represent oriented line-elements by oriented line-segments with a constant length (cf. Section 3.2).

For path planning in robotics (e.g. approximation, interpolation, optimization, ...) it is desirable to have a metric on $\overrightarrow{\mathcal{L}}$. Geometric meaningful metrics are investigated in Section 4. It turns out that two object dependent metrics are very suitable as they imply Euclidean metrics in the kinematic image space of a discussed point-model. Some basic results for their use in (variational) motion design are given in Section 5.1. Moreover, in Section 5.2 we adopt the famous algorithm of De Casteljau for Bézier curves for the motion design of oriented line-elements.

Before we can plunge in medias res we have to introduce some notations and basic concepts in Section 1.3.

1.3. Basics

A vector of $\mathbb{R}^3$ is denoted by $\mathbf{v} = (v_1, v_2, v_3)^T$ and the cross-product and Euclidean scalar-product of two vectors $\mathbf{v}, \mathbf{w} \in \mathbb{R}^3$ is denoted by $\mathbf{v} \times \mathbf{w}$ and $\langle \mathbf{v}, \mathbf{w} \rangle$, respectively.

Let $\mathbf{a}$ be the unit-vector in direction of the oriented line $\overrightarrow{\mathsf{a}}$, which is also known as spear, and $\mathbf{A}$ the position vector of $\mathsf{A} \in \mathsf{a}$. Then, the vector $\widehat{\mathbf{a}} := \mathbf{A} \times \mathbf{a}$ is the so-called moment vector and the bituple $(\mathbf{a}, \widehat{\mathbf{a}})$ of vectors in $\mathbb{R}^3$, which represents the so-called spear coordinates of $\overrightarrow{\mathsf{a}}$. Note that spear coordinates fulfill the equations

$$\langle \mathbf{a}, \mathbf{a} \rangle = 1, \quad \langle \mathbf{a}, \widehat{\mathbf{a}} \rangle = 0. \tag{3}$$

Moreover, we indicate dual numbers by an underline; i.e. $\underline{d} = d + \varepsilon \widehat{d}$ with $d, \widehat{d} \in \mathbb{R}$ and the dual unit ε having the property $\varepsilon^2 = 0$. These numbers constitute the commutative ring $\mathbb{D}$ of dual numbers. One can also define the extension of any real analytic function f to dual arguments as follows:

$$f(\underline{d}) := f(d) + \varepsilon \widehat{d} f'(d), \tag{4}$$

where f' denotes the derivative of f. For the sine and cosine function of the dual angle $\underline{\Phi} = \Phi + \varepsilon\widehat{\Phi}$ this yields:

$$\cos\underline{\Phi} = \cos\Phi - \varepsilon\widehat{\Phi}\sin\Phi \quad \in \mathbb{D}, \quad \sin\underline{\Phi} = \sin\Phi + \varepsilon\widehat{\Phi}\cos\Phi \quad \in \mathbb{D}. \tag{5}$$

Now we can map the spear coordinates $(\mathbf{a}, \widehat{\mathbf{a}})$ to an element of $\underline{\mathbf{a}} \in \mathbb{D}^3$ by $\underline{\mathbf{a}} := \mathbf{a} + \varepsilon\widehat{\mathbf{a}}$. Then, $\underline{\mathbf{a}}$ is a so-called dual unit-vector as

$$\langle\underline{\mathbf{a}}, \underline{\mathbf{a}}\rangle = \langle\mathbf{a}, \mathbf{a}\rangle + 2\varepsilon\langle\mathbf{a}, \widehat{\mathbf{a}}\rangle = 1 \tag{6}$$

holds due to Eq. (3). This implies Study's model of oriented lines (cf. [7, 16]):

Theorem 4. *There is a bijection between the set of oriented lines of $\mathbb{R}^3$ and the points on the dual unit-sphere $S^2_{\mathbb{D}} \in \mathbb{D}^3$.*

We proceed by introducing the notation of quaternions. $\mathfrak{Q} := q_0 + q_1\mathfrak{i} + q_2\mathfrak{j} + q_3\mathfrak{k}$ with $q_0, \ldots, q_3 \in \mathbb{R}$ is an element of the skew field of quaternions $\mathbb{H}$, where $\mathfrak{i}, \mathfrak{j}, \mathfrak{k}$ are the quaternion units, which are multiplied according to the following rules:

$$\mathfrak{ij} = -\mathfrak{ji} = \mathfrak{k}, \quad \mathfrak{jk} = -\mathfrak{kj} = \mathfrak{i}, \quad \mathfrak{ki} = -\mathfrak{ik} = \mathfrak{j}, \quad \mathfrak{ii} = \mathfrak{jj} = \mathfrak{kk} = -1.$$

It can be seen from this first formula that we write quaternions just side by side for multiplication instead of introducing an extra multiplication sign. This way the notation becomes more compact without yielding confusion as only quaternions are printed in Gothic. The quaternion conjugate to $\mathfrak{Q}$ is given by $\widetilde{\mathfrak{Q}} := q_0 - q_1\mathfrak{i} - q_2\mathfrak{j} - q_3\mathfrak{k}$. Moreover, a quaternion is called unit-quaternion if $\mathfrak{Q}\widetilde{\mathfrak{Q}} = 1$ holds.

Now we can also combine two quaternions $\mathfrak{Q}, \widehat{\mathfrak{Q}}$ by the dual unit to a so-called dual quaternion $\underline{\mathfrak{Q}} := \mathfrak{Q} + \varepsilon\widehat{\mathfrak{Q}}$. Obviously one will define the conjugate dual quaternion $\underline{\widetilde{\mathfrak{Q}}} := \widetilde{\mathfrak{Q}} + \varepsilon\widetilde{\widehat{\mathfrak{Q}}}$. Then, a dual unit-quaternion is defined as $\underline{\mathfrak{Q}}\,\underline{\widetilde{\mathfrak{Q}}} = 1$, which implies $\mathfrak{Q}$ to be a unit-quaternion and the so-called Study condition given in Eq. (1).

It is well-known (e.g. [15]) that the set of dual unit-quaternions yields a double cover of SE(3). The dual unit-sphere $S^3_{\mathbb{D}} \in \mathbb{D}^4$; i.e.

$$S^3_{\mathbb{D}} := \left\{\underline{\mathbf{Q}} := (q_0, q_1, q_2, q_3)^T + \varepsilon(\widehat{q}_0, \widehat{q}_1, \widehat{q}_2, \widehat{q}_3)^T \quad \text{with} \quad \langle\underline{\mathbf{Q}}, \underline{\mathbf{Q}}\rangle = 1\right\} \tag{7}$$

serves as a model for this double covering, where antipodal points imply the same spatial displacement. By homogenization we can avoid the double covering, which yields the Study parameters $(q_0 : q_1 : q_2 : q_3 : \widehat{q}_0 : \widehat{q}_1 : \widehat{q}_2 : \widehat{q}_3)$ already mentioned in Theorem 1. The displacement, which corresponds to a point on the Study quadric, can be written in matrix notation as $(x, y, z)^T \mapsto \mathbf{M}(x, y, z)^T + (t_1, t_2, t_3)^T$ with

$$\mathbf{M} = (m_{ij}) = \begin{pmatrix} q_0^2 + q_1^2 - q_2^2 - q_3^2 & 2(q_1q_2 - q_0q_3) & 2(q_1q_3 + q_0q_2) \\ 2(q_1q_2 + q_0q_3) & q_0^2 - q_1^2 + q_2^2 - q_3^2 & 2(q_2q_3 - q_0q_1) \\ 2(q_1q_3 - q_0q_2) & 2(q_2q_3 + q_0q_1) & q_0^2 - q_1^2 - q_2^2 + q_3^2 \end{pmatrix}, \tag{8}$$

and

$$t_1 = 2(q_0\widehat{q}_1 - q_1\widehat{q}_0 + q_2\widehat{q}_3 - q_3\widehat{q}_2), \quad t_2 = 2(q_0\widehat{q}_2 - q_2\widehat{q}_0 + q_3\widehat{q}_1 - q_1\widehat{q}_3), \quad t_3 = 2(q_0\widehat{q}_3 - q_3\widehat{q}_0 + q_1\widehat{q}_2 - q_2\widehat{q}_1),$$

if the normalizing condition $N = 1$ with $N := q_0^2 + q_1^2 + q_2^2 + q_3^2$ is fulfilled.

2. Point-models based on transformations

Three known approaches, which all have in common that they are based on rigid body motions, are studied/reviewed within the next subsections.

2.1. Incompletely specified displacements

One possibility for the description of $\overrightarrow{\mathcal{L}}$ is to ask for the set $\mathcal{D}$ of spatial Euclidean displacements SE(3), which map one oriented line-element $(\mathsf{B}, \overrightarrow{\mathsf{b}})$ into another one $(\mathsf{A}, \overrightarrow{\mathsf{a}})$. According to the notation of [17, 18] the displacement is not specified. More precisely, $\mathcal{D}$ is 1-dimensional, which can easily be seen as follows: Assume $\sigma \in \mathrm{SE}(3)$ with $\sigma(\mathsf{B}, \overrightarrow{\mathsf{b}}) = (\mathsf{A}, \overrightarrow{\mathsf{a}})$. Then, clearly also $\sigma(\rho(\mathsf{B}, \overrightarrow{\mathsf{b}})) = (\mathsf{A}, \overrightarrow{\mathsf{a}})$ holds, where ρ is an arbitrary rotation about the line b. As any element of $\mathcal{D}$ can be interpreted as a finite screw displacement due to Ball's theorem one can ask for the locus of the corresponding screw axes. It turned out [17, 18] that they generate the cylindroid, which is well-known from instantaneous kinematics. This "finite screw cylindroid" and the underlying set of finite screws (considered as 6-vectors; i.e. screw coordinates) were also studied in [19].

By modifying the definition of the finite screw's pitch (cf. [20]), the finite screws associated with $\mathcal{D}$ form a 2-system; i.e. any screw of this system can be represented by the linear combination of two basic screws (see also [21, 22, 23, 24]). This linear behavior also shows up by expressing $\mathcal{D}$ in terms of Study parameters as it corresponds to a line in the Study quadric (cf. [15, Section 11.3]). This observation is the starting point for our first point-model of $\overrightarrow{\mathcal{L}}$ resulting from the Grassmann coordinates of these lines:

For an efficient formulation of our problem in terms of dual quaternions, we use the result (cf. [25, Chapter 3, paragraph 1, item 3] that $\mathcal{D}$ contains at least one displacement δ, which is a pure rotation or translation. It is well-known that the corresponding dual quaternion $\underline{\mathfrak{D}}$ of δ can be written as

$$\underline{\mathfrak{D}} := \mathfrak{D} + \varepsilon\widehat{\mathfrak{D}} \quad \text{with} \quad \mathfrak{D} := d_0 + d_1\mathfrak{i} + d_2\mathfrak{j} + d_3\mathfrak{k} \quad \text{and} \quad \widehat{\mathfrak{D}} := \widehat{d_1}\mathfrak{i} + \widehat{d_2}\mathfrak{j} + \widehat{d_3}\mathfrak{k}. \tag{9}$$

Under the assumption that the identity transform (corresponding dual unit-quaternion is 1) maps the moving frame to the x-axis of the fixed frame (including orientation and origin; cf. end of Section 1.1) we get $\overrightarrow{\mathsf{b}} = \overrightarrow{\mathsf{x}}$. Therefore, the corresponding quaternion $\mathfrak{R}$ of ρ reads as $\mathfrak{R} = r_0 + r_1\mathfrak{i}$. The composite displacement is obtained by the multiplication $\underline{\mathfrak{D}}\mathfrak{R}$, which implies for $(r_0, r_1) = (1, 0)$ the following point on the Study quadric

$$U := (d_0 : d_1 : d_2 : d_3 : 0 : \widehat{d_1} : \widehat{d_2} : \widehat{d_3}), \tag{10}$$

and for $(r_0, r_1) = (0, 1)$ we get

$$V := (-d_1 : d_0 : d_3 : -d_2 : -\widehat{d_1} : 0 : \widehat{d_3} : -\widehat{d_2}). \tag{11}$$

As these two points are always distinct they span the line g in the Study quadric. Now we compute the 28 homogenous Grassmann coordinates $g_{ij} := u_i v_j - u_j v_i$ for $i < j$ and $i, j \in \{0, 1, \ldots, 7\}$:

$$g_{01} = d_0^2 + d_1^2 \qquad g_{23} = -d_2^2 - d_3^2 \tag{12}$$

$$g_{45} = \widehat{d_1}^2 \qquad g_{67} = -\widehat{d_2}^2 - \widehat{d_3}^2 \tag{13}$$

$$g_{02} = -g_{13} = d_0 d_3 + d_1 d_2 \qquad g_{03} = g_{12} = d_1 d_3 - d_0 d_2 \tag{14}$$

$$g_{04} = g_{15} = -d_0\widehat{d_1} \qquad g_{05} = -g_{14} = d_1\widehat{d_1} \tag{15}$$

$$g_{06} = -g_{17} = d_0\widehat{d_3} + d_1\widehat{d_2} \qquad g_{07} = g_{16} = d_1\widehat{d_3} - d_0\widehat{d_2} \tag{16}$$

$$g_{24} = -g_{35} = -d_2\widehat{d_1} \qquad g_{25} = g_{34} = -d_3\widehat{d_1} \tag{17}$$

$$g_{26} = g_{37} = d_2\widehat{d_3} - d_3\widehat{d_2} \qquad g_{27} = -g_{36} = -d_2\widehat{d_2} - d_3\widehat{d_3} \tag{18}$$

$$g_{46} = -g_{57} = \widehat{d_1}\widehat{d_2} \qquad g_{47} = g_{56} = \widehat{d_1}\widehat{d_3} \tag{19}$$

As there are 12 pairs of coordinates, which are identical or only differ by the sign we can project along these coordinates, thus we end up in the following 15-dimensional projective space $\mathbb{P}^{15}$:

$$(g_{01} : g_{02} : g_{03} : g_{04} : g_{05} : g_{06} : g_{07} : g_{23} : g_{24} : g_{25} : g_{26} : g_{27} : g_{45} : g_{46} : g_{47} : g_{67}). \tag{20}$$

Elimination of the variables $d_0, d_1, d_2, d_3, \widehat{d_1}, \widehat{d_2}, \widehat{d_3}$ from the equations given in Eqs. (12-19) yields a variety of dimension 6 and degree[2] 20. This variety has to be intersected with the hyperplane $g_{05} - g_{27} = 0$. The resulting 5-dimensional

[2]Based on the equations given in the Appendix, which determine this variety, the degree can easily be computed from the corresponding Hilbert-polynomial [26].

variety of degree 20 has to be sliced along the hyperplane $g_{01} - g_{23} = 0$ in order to get the final point-model for $\overrightarrow{\mathcal{L}}$ in $\mathbb{P}^{15}$, which is summed up next:

Theorem 5. *There exists a bijection between* $\overrightarrow{\mathcal{L}}$ *and all real points* $(g_{01} : g_{02} : g_{03} : g_{04} : g_{05} : g_{06} : g_{07} : g_{23} : g_{24} : g_{25} : g_{26} : g_{27} : g_{45} : g_{46} : g_{47} : g_{67})$ *of the* 15*-dimensional projective space* $\mathbb{P}^{15}$ *located on the* 5*-dimensional variety of degree 20, which is given by the set of equations displayed in the Appendix, and is sliced along the hyperplane* $g_{01} - g_{23} = 0$.

Note that the identity transform corresponds to the point $(1 : 0 : \ldots : 0)$ in the kinematic image space. This point-model possesses all three properties: P1 and P2 are trivially fulfilled, and P3 is implied by the Study quadric having this property.

Remark 2. Finally, we want to point out a flaw in [27, Proposition 2], where the following is claimed (translated to our terminology): "Every line within the Study quadric, which corresponds to a rigid displacement of an oriented line-element, has a unique intersection point with the hyperplane $q_1 = 0$ of Study's kinematic image space." This is not true as for $d_0 = d_1 = 0$ the complete line is located within the hyperplane $q_1 = 0$. Therefore, there is no bijection between this set of lines and a set of points in the hyperplane $q_1 = 0$, what violates the demanded property P2. ⋄

2.2. Point-model resulting from linear pentapods

For the study of the direct kinematics of a pentapod, where all platform anchor points are collinear, the following kinematic mapping has been used in [28]: Based on the Study parameters (cf. Section 1.3) the following nine equations can be defined:

$$n_0 = \widehat{d_0^2} + \widehat{d_1^2} + \widehat{d_2^2} + \widehat{d_3^2}, \quad y_0 = 4(-d_0\widehat{d_1} + d_1\widehat{d_0} + d_2\widehat{d_3} - d_3\widehat{d_2}) \tag{21}$$

$$x_0 = 2N, \quad x_i = 2m_{i,1}, \quad y_i = 2t_i \quad \text{for} \quad i = 1, 2, 3. \tag{22}$$

Then, eliminating the Study parameters from these nine equations together with the Study condition gives the following result:

Theorem 6. *There exists a bijection between* $\overrightarrow{\mathcal{L}}$ *and all real points* $(n_0 : x_0 : \ldots : x_3 : y_0 : \ldots : y_3)$ *of the* 8*-dimensional projective space* $\mathbb{P}^8$ *located on the* 5*-dimensional octic variety given by*

$$x_1^2 + x_2^2 + x_3^2 - x_0^2 = 0, \quad y_1^2 + y_2^2 + y_3^2 - 8x_0n_0 = 0, \quad x_0y_0 + x_1y_1 + x_2y_2 + x_3y_3 = 0, \tag{23}$$

which is sliced along the hyperplane $x_0 = 0$.

For $x_0 = 1$ the Euclidean displacement of $(\mathsf{B}, \overrightarrow{\mathsf{b}}) \mapsto (\mathsf{A}, \overrightarrow{\mathsf{a}})$ is given by:

$$\mathbf{B} = \begin{pmatrix} b_0 \\ 0 \\ 0 \end{pmatrix} \mapsto \begin{pmatrix} b_0x_1 + y_1 \\ b_0x_2 + y_2 \\ b_0x_3 + y_3 \end{pmatrix} = \mathbf{A} \quad \text{and} \quad \mathbf{b} = \begin{pmatrix} 1 \\ 0 \\ 0 \end{pmatrix} \mapsto \begin{pmatrix} x_1 \\ x_2 \\ x_3 \end{pmatrix} = \mathbf{a}. \tag{24}$$

Note that the variables y_0 and n_0 were only introduced for the special application in robotics, as then the so-called sphere condition is only linear in the nine homogenous motion parameters $(n_0 : \ldots : y_3)$. As seen in Eq. (24), y_0 and n_0 do not play a role in the transformation, thus we can omit these two unknowns. This yields the following simplified point-model:

Theorem 7. *There exists a bijection between* $\overrightarrow{\mathcal{L}}$ *and all real points* $(x_0 : x_1 : x_2 : x_3 : y_1 : y_2 : y_3)$ *of the* 6*-dimensional projective space* $\mathbb{P}^6$ *located on the* 5*-dimensional singular quadric*

$$x_1^2 + x_2^2 + x_3^2 - x_0^2 = 0, \tag{25}$$

which is sliced along the hyperplane $x_0 = 0$.

For both point-models (cf. Theorems 6 and 7) it can be verified that they possess the three properties P1, P2 and P3. The proof is left to the interested reader.

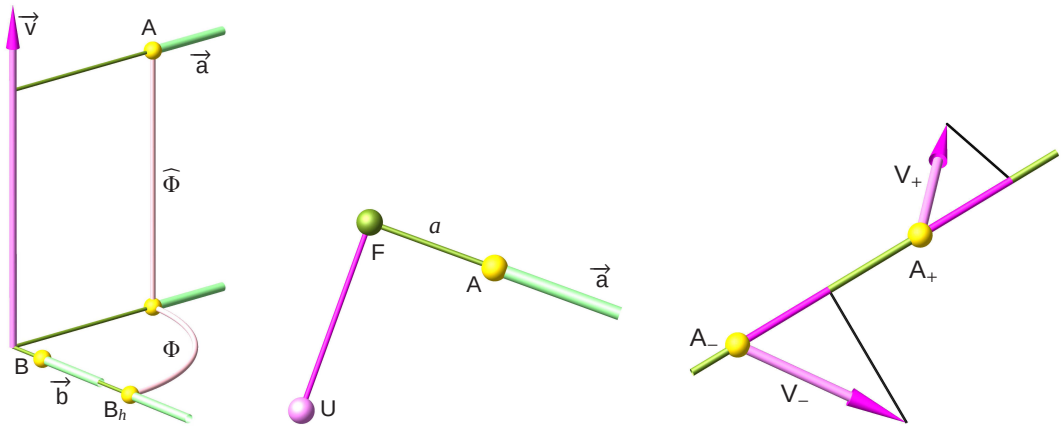

Figure 3: Left: Geometric interpretation of the displacement operator. Middle: Illustration of the oriented distance a. Right: Illustration of the Projection Theorem.

2.3. Displacement operators of Zhang and Ting

The last approach of this section is based on the following theorem [2, Theorem 1]:

Theorem 8. *For any oriented line-element* $(\mathsf{B}, \vec{\mathsf{b}})$ *there exists a bijection between* $\vec{\mathcal{L}}$ *and the set* O *of its displacement operators, which is given by*

$$O := \left\{(1+\varepsilon h)(\cos\underline{\Phi}, \underline{\mathbf{v}}\sin\underline{\Phi}) \quad \textit{with} \quad \langle \underline{\mathbf{b}}, \underline{\mathbf{v}}\rangle = 0 \quad \textit{and} \quad \langle \underline{\mathbf{v}}, \underline{\mathbf{v}}\rangle = 1\right\}. \tag{26}$$

The geometric interpretation of the displacement operators[3] is as follows (see Figure 3 (left)): $\underline{\mathbf{v}}$ represents an oriented line $\vec{\mathsf{v}}$, which intersects $\vec{\mathsf{b}}$ orthogonally due to the condition $\langle \underline{\mathbf{b}}, \underline{\mathbf{v}}\rangle = 0$. Applying the displacement operator to $(\mathsf{B}, \vec{\mathsf{b}})$ yields a translation of B along $\vec{\mathsf{b}}$ by the oriented distance h, then the resulting oriented line-element $(\mathsf{B}_h, \vec{\mathsf{b}})$ is rotated about $\vec{\mathsf{v}}$ by the oriented angle Φ and translated along $\vec{\mathsf{v}}$ by the oriented distance $\widehat{\Phi}$ into its final pose $(\mathsf{A}, \vec{\mathsf{a}})$. The last two transformations can be seen as a screw displacement about the axis $\vec{\mathsf{v}}$, which is the (oriented) common perpendicular of $\vec{\mathsf{a}}$ and $\vec{\mathsf{b}}$, respectively.

By expanding the displacement operator given in Theorem 8 with respect to $\underline{\Phi} := \Phi + \varepsilon\widehat{\Phi}$ and Eq. (5) yields:

$$(1+\varepsilon h)[\underbrace{(\cos\Phi, \mathbf{v}\sin\Phi)}_{(e_0,\mathbf{e})} + \varepsilon\underbrace{(-\widehat{\Phi}\sin\Phi, \widehat{\mathbf{v}}\sin\Phi + \mathbf{v}\widehat{\Phi}\cos\Phi)}_{(\widehat{e}_0,\widehat{\mathbf{e}})}]. \tag{27}$$

$h, \underline{\Phi}, \underline{\mathbf{v}}$ with $\langle \underline{\mathbf{b}}, \underline{\mathbf{v}}\rangle = 0$ are no suitable parameters for an algebraic description of O as from Eq. (27) it can be seen that for $\sin\Phi = 0$ the vector $\widehat{\mathbf{v}}$ can be arbitrary. Moreover, for $h, -\underline{\Phi}, -\underline{\mathbf{v}}$ and $h, \underline{\Phi}, \underline{\mathbf{v}}$ we get the same displacement operator. This problem can be avoided by considering the parameters $e_0, \widehat{e}_0, \mathbf{e}, \widehat{\mathbf{e}}, h$ (cf. Eq. (27)) and by replacing the condition $\langle \underline{\mathbf{b}}, \underline{\mathbf{v}}\rangle = 0$ by:

$$\langle \mathbf{e}, \mathbf{b}\rangle = \langle \mathbf{v}, \mathbf{b}\rangle \sin\Phi = 0 \quad \text{and} \quad \langle \widehat{\mathbf{e}}, \mathbf{b}\rangle + \langle \widehat{\mathbf{b}}, \mathbf{e}\rangle = \left(\langle \widehat{\mathbf{v}}, \mathbf{b}\rangle + \langle \widehat{\mathbf{b}}, \mathbf{v}\rangle\right)\sin\Phi + \langle \mathbf{v}, \mathbf{b}\rangle\widehat{\Phi}\cos\Phi = 0. \tag{28}$$

By assumption that the identity transform (corresponding displacement operator is 1) maps the moving frame to the x-axis of the fixed frame (including orientation and origin; cf. end of Section 1.1) we get $\vec{\mathsf{b}} = \vec{\mathsf{x}}$. This simplifies Eq. (28) to $e_1 = \widehat{e}_1 = 0$, which already shows the following theorem:

[3] In [2] the displacement operator is given as a dual quaternion instead of an element of $\mathbb{D}^4$ (cf. Section 1.3), which is chosen for convenience within the study at hand.

Theorem 9. *There exists a bijection between* $\overrightarrow{\mathcal{L}}$ *and all real points* $(e_0, e_2, e_3, \widehat{e}_0, \widehat{e}_2, \widehat{e}_3, h)$ *of the* 7*-dimensional space* $\mathbb{R}^7$ *located on the* 5*-dimensional quartic variety given by*

$$e_0\widehat{e}_0 + e_2\widehat{e}_2 + e_3\widehat{e}_3 = 0, \quad e_0^2 + e_2^2 + e_3^2 = 1. \tag{29}$$

Note that the identity transform corresponds to the point $(1, 0, \ldots, 0)$ in the kinematic image space. This point-model possesses P1 and P2 but not P3, which can be seen as follows:

The operator, which transforms the oriented line-element $(\mathsf{U}, \overrightarrow{\mathsf{x}})$ into $(\mathsf{A}, \overrightarrow{\mathsf{a}})$, is given by

$$(e_0, e_2, e_3, \widehat{e}_0, \widehat{e}_2, \widehat{e}_3, h) := (a_1, -a_3, a_2, \widehat{a}_1, -\widehat{a}_3, \widehat{a}_2, h_A) \tag{30}$$

with

$$h_A = \frac{a_2\widehat{a}_3 - a_2\widehat{a}_3}{1 + a_1} + a, \tag{31}$$

where a denotes the distance from the pedal point F of a (with respect to the origin U of the fixed frame) to the point A with respect to the orientation of a; i.e. a is an oriented distance (see Figure 3 (middle)).

Now we change the fixed frame, which is equivalent to moving the line-element $(\mathsf{A}, \overrightarrow{\mathsf{a}})$. For showing the non-linear transform of the point-model of Theorem 9, we can even restrict to translations by an arbitrary vector $(x, y, z)^T$. Then, a straight forward computation yields:

$$(e_0', e_2', e_3', \widehat{e}_0', \widehat{e}_2', \widehat{e}_3', h') := (e_0, e_2, e_3, \widehat{e}_0 - ye_2 - ze_3, \widehat{e}_2 - xe_3 + ye_0, \widehat{e}_3 + xe_3 + ze_0, h_A') \tag{32}$$

with

$$h_A' = \frac{e_3 y + e_2 z}{1 + e_0} + x + h_A. \tag{33}$$

This shows that h_A' cannot be represented as a linear combination of $(e_0, e_2, e_3, \widehat{e}_0, \widehat{e}_2, \widehat{e}_3, h)$. Note that the problem is only the transform of h; the remaining coordinates transform linearly also in the general case (not restricted to translations).

Remark 3. Finally, it should be noted that one can also transform the oriented line-element $(\mathsf{U}, \overrightarrow{\mathsf{x}})$ into $(\mathsf{A}, \overrightarrow{\mathsf{a}})$ just by a screw motion (angle Φ and translation $\widehat{\Phi}$), where the axis $\overrightarrow{\mathsf{w}}$ is orthogonal to $\overrightarrow{\mathsf{x}}$ (and $\overrightarrow{\mathsf{a}}$). One can encode this screw analogously to Eq. (26), which yields

$$(\cos\underline{\Phi}, \underline{\mathbf{w}}\sin\underline{\Phi}) \quad \text{with} \quad \langle \mathbf{x}, \mathbf{w}\rangle = 0 \quad \text{and} \quad \langle \underline{\mathbf{w}}, \underline{\mathbf{w}}\rangle = 1,$$

thus one gets rid of the parameter h. This implies a similar point-model as in Theorem 9; but it also does not possess P3, which can be seen in a similar way as above. ◇

3. Point-models based on representations

3.1. Representations of oriented line-elements

The representations of oriented line-elements can be grouped into three approaches:

3.1.1. Representation of Odehnal, Pottmann, Wallner

In [29] the three authors study unoriented line-elements of $\mathbb{R}^3$. Their result can be adapted for oriented ones by adding a normalization condition, which results in the following point-model:

Theorem 10. *There exists a bijection between* $\overrightarrow{\mathcal{L}}$ *and all real points* $(\mathbf{a}, \widehat{\mathbf{a}}, a)$ *of the* 7*-dimensional space* $\mathbb{R}^7$ *located on the* 5*-dimensional quartic variety given by*

$$\langle \mathbf{a}, \mathbf{a}\rangle = 1, \quad \langle \mathbf{a}, \widehat{\mathbf{a}}\rangle = 0. \tag{34}$$

Remark 4. The point-model can be seen as a cylinder over the Study model of oriented lines (cf. Theorem 4). ◇

This point-model resulting from a representation can be interpreted in terms of displacements as follows: The identity transform is given by $(1, 0, \ldots, 0)$. Any other point of the point-model describes the relative position of $(\mathsf{U}_0, \overrightarrow{\mathsf{x}}_0)$ with respect to the fixed frame $\mathcal{F}$.

P1 and P2 are trivially fulfilled. The third property with respect to changes of the fixed frame follows from [29, Eq. (8)]. Moreover, changes of the moving frame only imply a translation of the point on the oriented line; i.e. a transforms linearly to $a + t$ with $t \in \mathbb{R}$.

3.1.2. Representation of Selig and Odehnal

Based on Clifford algebras (cf. [1, 15, 30]), oriented line-elements are just represented by combining grade 2 elements (oriented lines) with grade 4 elements (points) under the side condition that the point is located on the oriented line. This is similar to the approach of Odehnal [31] taken for characterizing unoriented line-elements of $\mathbb{P}^3$. Therefore, these two approaches imply the same point-model for $\overrightarrow{\mathcal{L}}$:

Theorem 11. *There exists a bijection between* $\overrightarrow{\mathcal{L}}$ *and all real points* $(\mathbf{a}, \widehat{\mathbf{a}}, \mathbf{A})$ *of the* 9*-dimensional space* $\mathbb{R}^9$ *located on the* 5*-dimensional variety of degree* 10 *given by*

$$\langle \mathbf{a}, \mathbf{a} \rangle = 1, \quad \langle \mathbf{a}, \widehat{\mathbf{a}} \rangle = 0, \quad \langle \mathbf{A}, \widehat{\mathbf{a}} \rangle = 0, \quad \mathbf{A} \times \mathbf{a} = \widehat{\mathbf{a}}. \tag{35}$$

The degree of 10 follows from [31, Theorem 3.1] under consideration of the additional constraint $\langle \mathbf{a}, \mathbf{a} \rangle = 1$.

The interpretation of this point-model in terms of displacements can be done as in Section 3.1.1. Again P1 and P2 are trivially fulfilled. The third property with respect to changes of the fixed frame follows from [31, Eq. (12)]. Moreover, changes of the moving frame imply again a translation of the point on the line; i.e. $\mathbf{A}$ transforms linearly to $\mathbf{A} + \mathbb{R}\mathbf{a}$.

3.1.3. The trivial representation and those of Zhang and Ting, Combebiac

The most intuitive approach for representing an oriented line-element is just to combine the point coordinates $\mathbf{A}$ and the unit-direction-vector $\mathbf{a}$ of $\overrightarrow{\mathsf{a}}$. This yields the following theorem:

Theorem 12. *There exists a bijection between* $\overrightarrow{\mathcal{L}}$ *and all real points* $(\mathbf{a}, \mathbf{A})$ *of the* 6*-dimensional space* $\mathbb{R}^6$ *located on the singular quadric*

$$\langle \mathbf{a}, \mathbf{a} \rangle = 1. \tag{36}$$

Note that this point-model can be seen as the non-homogenous version of the one given in Theorem 7.

Zhang and Ting [2] represented oriented line-elements by the 6-tuple

$$(\mathbf{a}, \widehat{\mathbf{a}} + a\mathbf{a}), \tag{37}$$

where a denotes the oriented distance illustrated in Figure 3 (middle).

A similar description is used by Combebiac [32]:

$$(\mathbf{a}, \widehat{\mathbf{a}} + \mathbf{A}). \tag{38}$$

For both representations it can easily be seen that their implied point-model is given by the same singular quadric of Theorem 12. But it should be mentioned that the transform between these three point-models (in all three cases) is a non-linear one.

For all three point-models it can be verified that they possess the three properties P1, P2 and P3. The proof is left to the reader, where the interpretation of these point-models in terms of displacements can be done as in Section 3.1.1 as well.

3.2. Representations of oriented line-segments with a constant length

The idea is to represent an oriented line-segment by an ordered pair $(\mathsf{A}_-, \mathsf{A}_+)$ of points A_- and A_+. If we additionally demand that the distance between these two points equals a constant value $d > 0$ we can come up with the following bijection between the set of oriented line-elements with constant length d and $\overrightarrow{\mathcal{L}}$. The oriented axis $\overrightarrow{\mathsf{a}}$ is given by $\overrightarrow{\mathsf{A}_-\mathsf{A}_+}$ and the point A is given by $\mathsf{A}_- + \lambda\overrightarrow{\mathsf{A}_-\mathsf{A}_+}$ for a fixed $\lambda \in \mathbb{R}$.

From the applicational point of view two possibilities are reasonable:

1. If the rotational end-effector has a second remarkable point beside the tool tip A, then these two points can be regarded as A_+ and A_-, respectively (with $\lambda = 0$). One might think of the following examples:
   - If the tool axis contains the wrist of a 6R-robot, then this special point can be chosen as A_+.
   - If the end-effector is a miller, then the second endpoint can be considered as A_+ (see Figure 4 (left)).
2. Another geometric meaningful choice is to select A_- and A_+ in a way on $\overrightarrow{\mathsf{a}}$ that A is their midpoint ($\Rightarrow \lambda = \frac{1}{2}$). In this case we still have the free choice of d (see Figure 4 (right)).

Figure 4: Two reasonable possibilities for representing an oriented line-element by an oriented line-segment.

3.2.1. Representations of Wang, Ge and Ravani

In [33, 34] the authors propose the following representations:

1. In [33] an "augmented unit line vector" is introduced by the following definition:

$$(\mathbf{a}, \widehat{\mathbf{a}}, a_-, a_+) \quad \text{with} \quad \langle \mathbf{a}, \mathbf{A}_- \rangle = a_- \quad \text{and} \quad \langle \mathbf{a}, \mathbf{A}_+ \rangle = a_+. \tag{39}$$

   As the entries a_-, a_+ are ordered, we can even homogenize this 8-tuple, which implies the following point-model:

   Theorem 13. *There exists a bijection between* $\overrightarrow{\mathcal{L}}$ *and all real points* $(\mathbf{a} : \widehat{\mathbf{a}} : a_- : a_+)$ *of the* 7*-dimensional projective space* $\mathbb{P}^7$ *located on the* 5*-dimensional quartic given by*

$$\langle \mathbf{a}, \widehat{\mathbf{a}} \rangle = 0, \quad (a_- - a_+)^2 = d^2 \langle \mathbf{a}, \mathbf{a} \rangle, \tag{40}$$

   which is sliced along the 4*-dimensional plane* $a_1 = a_2 = a_3 = 0$.

   This point-model can be regarded as the homogenized version of the one given in Theorem 10, and therefore the holding of the three properties P1, P2 and P3 can be reasoned analogously.

2. As the orientation of the line-segment is given by $\overrightarrow{\mathsf{A}_-\mathsf{A}_+}$, one can assume that $\mathbf{a}$ is oriented in a way that $a_+ > a_-$ holds (cf. [34, Section 1.2]). Then, we get the following connection:

$$d = a_+ - a_-, \quad a = (a_- + a_+)/2. \tag{41}$$

   Thus, we can rewrite Eq. (39) by the 8-tuple $(\mathbf{a}, \widehat{\mathbf{a}}, a, d)$. As d is a constant, we can omit it and end up with exactly the same point-model given in Theorem 10.

3. Moreover, Ravani and Ge [34, Section 1.3] suggested to use the representation $(d + \varepsilon a)\underline{\mathbf{a}}$. For[4] $d = 1$ this is equivalent with the already discussed representation given in Eq. (37).

4. Finally, they proposed in [34, Section 1.4] to represent a line-segment by a finite screw as point on $S^3_{\mathbb{D}} \in \mathbb{D}^4$ (cf. Eq. (7)):

$$(\cos \underline{\Psi}, \sin \underline{\Psi}\, \underline{\mathbf{a}}) \quad \text{with} \quad \underline{\Psi} = \Psi + \varepsilon \widehat{\Psi}. \tag{42}$$

   Based on the used definition for the pitch we end up with the following two models:

[4] We can rescale the Euclidean 3-space in a way that the distance d between A_- and A_+ equals one. Note that this can be done without loss of generality as it is just a matter of defining the unit length.

(a) Using the standard definition of the pitch yields $\widehat{\Psi} = a$ and $\Psi = \arctan d$. By setting $d = 1$ (cf. footnote 4) the expression of Eq. (42) simplifies to:

$$\tfrac{\sqrt{2}}{2}[(1, \underbrace{\mathbf{a}}_{\mathbf{e}}) + \varepsilon(\underbrace{-a}_{\widehat{e}}, \underbrace{\widehat{\mathbf{a}} + a\mathbf{a}}_{\widehat{\mathbf{e}}})]. \tag{43}$$

This implies the following point-model:

Theorem 14. *There exists a bijection between* $\overrightarrow{\mathcal{L}}$ *and all real points* $(\mathbf{e}, \widehat{\mathbf{e}}, \widehat{e})$ *of the* 7*-dimensional space* $\mathbb{R}^7$ *located on the* 5*-dimensional quartic given by*

$$\langle \mathbf{e}, \mathbf{e} \rangle = 1, \quad \langle \mathbf{e}, \widehat{\mathbf{e}} \rangle + \widehat{e} = 0. \tag{44}$$

The coordinates of this point-model can be regarded as the representation of Zhang and Ting given in Eq. (37) augmented by the coordinate $\widehat{e} = -a$. Therefore, it is clear that also this point-model possesses all three properties.

(b) Using the pitch definition of Parkin [20] with $\widehat{\Psi} = a$ and $\Psi = 2 \arctan \frac{d}{2}$, we get the following result for Eq. (42) under consideration of $d = 2$ (cf. footnote 4):

$$(0, \mathbf{a}) + \varepsilon(-a, \widehat{\mathbf{a}}). \tag{45}$$

The same procedure as in (i) yields the point-model of Theorem 10 (up to the sign of a).

3.2.2. Representation of Chen and Pottmann

In [35] a line-segment is represented by their endpoints; i.e. $(\mathbf{A}_-, \mathbf{A}_+)$. This implies the following point-model:

Theorem 15. *There exists a bijection between* $\overrightarrow{\mathcal{L}}$ *and all real points* $(\mathbf{A}_-, \mathbf{A}_+)$ *of the* 6*-dimensional space* $\mathbb{R}^6$ *located on the singular hyperquadric*

$$\Omega: \quad < \mathbf{A}_- - \mathbf{A}_+, \mathbf{A}_- - \mathbf{A}_+ \rangle = d^2. \tag{46}$$

This point-model can be obtained by a linear transformation of the one given in Theorem 12. Therefore, it also possesses the three properties P1, P2 and P3.

4. Metric aspects

As already mentioned in Section 1.2 it is desirable for path planning in robotics (e.g. approximation, interpolation, optimization, ...) to have a metric f on $\overrightarrow{\mathcal{L}}$; i.e. the point-model together with f form a metric space.

One can come up with the idea to use geometric meaningful motion-parameters of the transform $(\mathsf{B}, \overrightarrow{\mathsf{b}}) \mapsto (\mathsf{A}, \overrightarrow{\mathsf{a}})$ for the definition of a metric. For the displacement operator of Zhang and Ting (cf. Section 2.3) a distance between two oriented line-elements can be defined based on a Riemannian metric on SE(3) by $\sqrt{c_1\Phi^2 + c_2(\widehat{\Phi}^2 + h^2)}$, where c_1, c_2 are some positive scalars (cf. [36]). For the transform mentioned in Remark 3 analogous considerations yield $\sqrt{c_1\Phi^2 + c_2\widehat{\Phi}^2}$. Note that these metrics are only invariant with respect to the change of the fixed frame (but not with respect to the moving frame).

These distance metrics on SE(3) are quite problematic as they depend on the choice of length and angle scales as already pointed out by Park [37]. He also mentioned an alternative to this approach by changing the point of view as follows: Instead of a distance metric on SE(3) one can consider the distance between two configurations of the same rigid body, which yields so-called object dependent metrics firstly studied by Kazerounian and Rastegar [38]. This interpretation suggests to consider an oriented line-element as an oriented line-segment with a constant length d.

The following geometric meaningful object dependent metrics occur already in the literature:

4.1. Metric of Kazerounian and Rastegar

Their metric proposed in [38, Section 3.1] reads as follows modified for the problem under consideration

$$\frac{1}{d}\int_{\mathsf{X}\in\overline{\mathsf{B}_-\mathsf{B}_+}} \kappa(\mathbf{X})\|\mathbf{X}-\delta(\mathbf{X})\|^2, \tag{47}$$

where δ denotes the displacement $(\mathsf{B}_-,\mathsf{B}_+)\mapsto(\mathsf{A}_-,\mathsf{A}_+)$ and $\kappa(\mathbf{X})$ is a weight function, which can be used to consider the mass distribution within the object. Direct computation shows that under the assumption of a unit mass distribution $\kappa(\mathbf{X})=1$ the distance measure of Eq. (47) equals the metric suggested by Chen and Pottmann [35], which is given by[5]

$$f_1(\mathcal{A},\mathcal{B})^2 := \tfrac{1}{3}\left[(\mathbf{A}_- - \mathbf{B}_-)^2 + (\mathbf{A}_+ - \mathbf{B}_+)^2 + (\mathbf{A}_- - \mathbf{B}_-)(\mathbf{A}_+ - \mathbf{B}_+)\right] \tag{48}$$

with $\mathcal{A} := (\mathbf{A}_-,\mathbf{A}_+)$ and $\mathcal{B} := (\mathbf{B}_-,\mathbf{B}_+)$. Moreover, it is advantageous to combine this metric with the point-model of Theorem 15 as it implies a Euclidean metric in the kinematic image space $\mathbb{R}^6$ induced by the positive-definite quadratic form

$$\langle C,C\rangle_1 = \tfrac{1}{3}\left[\langle\mathbf{C}_-,\mathbf{C}_-\rangle + \langle\mathbf{C}_+,\mathbf{C}_+\rangle + \langle\mathbf{C}_-,\mathbf{C}_+\rangle\right] \tag{49}$$

with $C := \mathcal{A}-\mathcal{B}$.

Remark 5. Note that the metric of Kazerounian and Rastegar is originally defined only for points on Ω of Eq. (46), but due to the equivalence with the metric proposed by Chen and Pottmann [35] it can be extended to the complete kinematic image space $\mathbb{R}^6$. Finally, it should be mentioned that this metric has been used in [39] for optimizing 5-axis machining, where it has been erroneously interpreted as the area of the surface patch (hyperbolic paraboloid or plane) spanned by $\mathcal{A}$ and $\mathcal{B}$. ◇

4.2. Metric of Pottmann, Hofer and Ravani

The idea of the following metric given in [40] is based on the so-called registration problem with known correspondences. One samples a number n of points $\mathsf{X}_1,\ldots,\mathsf{X}_n$ from the surface of the moving object (e.g. by laser scanning) and defines the squared distance between two of its poses by the sum of the squared distances of the n corresponding point pairs.

Remark 6. As this distance strongly depends on the number n of points we suggest to divide the sum by n; this corresponds to the mean of the squared distances of the n point pairs. ◇

As in our case the rigid body is only 1-dimensional, its boundary is just given by the two end points A_- and A_+, respectively. Consequently, the distance function f_2 between two line-segments (under consideration of Remark 6) is given by

$$f_2(\mathcal{A},\mathcal{B})^2 := \tfrac{1}{2}\left[(\mathbf{A}_- - \mathbf{B}_-)^2 + (\mathbf{A}_+ - \mathbf{B}_+)^2\right]. \tag{50}$$

This metric also makes sense between line-segments of different lengths. Therefore, we can extend it from Ω to the ambient space $\mathbb{R}^6$ of the point-model given in Theorem 15. Clearly $\mathbb{R}^6$ equipped with f_2 is again a Euclidean space and the corresponding positive-definite quadratic form is given by

$$\langle C,C\rangle_2 = \tfrac{1}{2}\left[\langle\mathbf{C}_-,\mathbf{C}_-\rangle + \langle\mathbf{C}_+,\mathbf{C}_+\rangle\right]. \tag{51}$$

Remark 7. The geometric interpretation of $f_i(\mathcal{A},\mathcal{B})^2$ is as follows: $f_i(\mathcal{A},\mathcal{B})^2$ is the mean of the squared distances of corresponding points over the entire line-segment (case f_1) resp. of the boundary of the line-segment (case f_2). For line-segments of the same length d the difference $f_2(\mathcal{A},\mathcal{B})^2 - f_1(\mathcal{A},\mathcal{B})^2$ is given by $\frac{1}{3}d^2(1-\cos\sphericalangle(\vec{\mathsf{a}},\vec{\mathsf{b}}))$. Thus, for $\sphericalangle(\vec{\mathsf{a}},\vec{\mathsf{b}})=0$ both distance metrics are identical and for $\sphericalangle(\vec{\mathsf{a}},\vec{\mathsf{b}})=\pi$ they have the greatest possible deviation of $\frac{2}{3}d^2$.

Clearly one can also think of combining these two metrics to $f_\mu := \mu_1 f_1 + \mu_2 f_2$, where μ_1 and μ_2 have to be chosen in a way that the corresponding quadratic form is positive-definite. ◇

[5] In [35] it is originally defined without the factor $\frac{1}{3}$, but this was just done for convenience.

5. Motion design

The most relevant problem in motion design is the so-called motion interpolation problem, which can be stated as follows: Given a number k of interpolate poses $(\mathsf{A}^i, \overrightarrow{\mathsf{a}}^i)$ for $i = 1, \ldots, k$ of the oriented line-element $(\mathsf{A}, \overrightarrow{\mathsf{a}})$, compute an interpolating motion through the ordered sequence of interpolate poses. For all outlined point-models, which are quadrics in the kinematic image space, one can use the following two known methods:

- rational interpolation of points on hyperquadrics [41],
- interpolation with rational quadratic spline curves (biarc construction) [42].

Note that their application to the Study quadric was already done in [12, 13]. Further interpolation methods for oriented line-elements, which are known to the author, read as follows:

- In [27] one identifies the first pose $(\mathsf{A}^1, \overrightarrow{\mathsf{a}}^1)$ (= reference pose) with the identity transform and the other poses $(\mathsf{A}^i, \overrightarrow{\mathsf{a}}^i)$ for $i = 2, \ldots, k$ with the dual quaternions $\underline{\mathfrak{D}}_i$ according to Remark 2 (assumed they are uniquely defined). Then, these points $1, \underline{\mathfrak{D}}_2, \ldots, \underline{\mathfrak{D}}_k$ are interpolated by a NURBS curve. Note that the resulting interpolant depends on the selection of the reference pose.
- Based on the representation given in Theorem 15, which has also been used in the patent [43], the computation of a NURBS interpolant (within the machining tolerance) is outlined in [44].
- In [45] the positioning of the tool tip and the orientation of the tool axis are separated. Therefore, they computed near arc-length parametrized quintic polynomial splines and near arc-length parametrized quintic spherical Bézier curves, respectively. In order to synchronize the position and orientation splines at the control poses they used a so-called reparametrization spline.

Remark 8. If we pick up the idea in separating the computation of orientation and positioning, one can also use other methods for the orientation interpolation as e.g. [46, 47, 48] and then compute the interpolating translational motion in a way that the composite motion contains all control poses. ◇

5.1. Variational motion design

In the following we want to focus on the (variational) motion design algorithm proposed in [40], which can be adapted to the path planing of oriented line-elements, based on the object depended metrics in the kinematic image space of Chen and Pottmann (cf. Section 3.2.2). This algorithm can be summarized as follows:

Step 1 Interpolate the given poses by a linear curve design algorithm in $\mathbb{R}^6$, which yields the interpolating curve $\mathsf{c} \in \mathbb{R}^6$.

Step 2 Project c orthogonally onto Ω (projection ω), which already yields an interpolating motion $\omega(\mathsf{c})$.

Step 3 In addition, one can use this interpolating motion $\omega(\mathsf{c})$ as a starting point for the computation of an energy-minimizing motion. For this we have to discretize $\omega(\mathsf{c})$ into a poly-line with vertex set $\{\mathsf{P}_1, \ldots, \mathsf{P}_K\}$ containing the control poses. Then, we run the following iterative algorithm:

(a) Move each P_i, which is no control pose, within the tangent space to Ω in a way that the discretized energy-functional gets minimal. For a geodesic motion we have to minimize

$$E_g = \sum_{i=1}^{K-1} \langle \mathcal{P}_{i+1} - \mathcal{P}_i, \mathcal{P}_{i+1} - \mathcal{P}_i \rangle_j \tag{52}$$

and for a motion with a minimal bending energy the following function

$$E_b = \sum_{i=1}^{K-2} \langle (\mathcal{P}_{i+2} - \mathcal{P}_{i+1}) - (\mathcal{P}_{i+1} - \mathcal{P}_i), (\mathcal{P}_{i+2} - \mathcal{P}_{i+1}) - (\mathcal{P}_{i+1} - \mathcal{P}_i) \rangle_j \tag{53}$$

where $j = 1, 2$ refers to the underlying metric.

(b) Project the obtained points (minimizer) back onto Ω by ω.

Steps (a) and (b) are done iteratively under consideration of a clever step-size selection as long as the sum of the squared distances of corresponding vertices of two consecutive poly-lines drops below a certain threshold value. The choice of the scalar-product does not play a role for the outcome of this algorithm as also the minimizer of step 3(a) is for both scalar-products (or any scalar-product $\langle .,. \rangle_\mu$ associated with f_μ of Remark 7) the same, which can easily be seen. Clearly one can also minimize a combination of E_g and E_b.

A very detailed description of this algorithm, which can also be modified in order to avoid obstacles, is given by Hofer [49], but it is also briefly outlined in [50].

Remark 9. If one wants to have a rational representation, one can interpolate/approximate the final poly-line of the above algorithm by B-spline curves as done in [44] or by a higher dimensional version of the method proposed in [51]. For the latter approach one needs a parametrization of Ω, which for example can be given as follows:

$$(\mathbf{A}_-, \mathbf{A}_- + d\mathbf{a}) \quad \text{with} \quad \mathbf{a} := \left(\frac{2p_1}{1+p_1^2+p_2^2}, \frac{2p_2}{1+p_1^2+p_2^2}, \frac{p_1^2+p_2^2-1}{1+p_1^2+p_2^2} \right) \tag{54}$$

with the five parameters $(\mathbf{A}_-, p_1, p_2) \in \mathbb{R}^5$. ◇

In order to perform the above outlined algorithm the only missing ingredients are the orthogonal projection ω and the knowledge of the instantaneous motions of a line-segment with constant length, which form the tangent space to Ω. These two little gaps are closed next:

Theorem 16. *Given is a point $\mathcal{A} = (\mathbf{A}_-, \mathbf{A}_+) \in \mathbb{R}^6 \setminus \Omega$ with $\mathbf{A}_- \neq \mathbf{A}_+$. Then, the closest point $\mathcal{B} = (\mathbf{B}_-, \mathbf{B}_+) \in \Omega$ with respect to both distance measures $f_i(\mathcal{A}, \mathcal{B})^2$ for $i = 1, 2$ is given by:*

$$\left(\frac{\mathbf{A}_- + \mathbf{A}_+}{2} - \frac{d}{2}\mathbf{a}, \frac{\mathbf{A}_- + \mathbf{A}_+}{2} + \frac{d}{2}\mathbf{a} \right) \quad \textit{with} \quad \mathbf{a} = \frac{\mathbf{A}_+ - \mathbf{A}_-}{\|\mathbf{A}_+ - \mathbf{A}_-\|}. \tag{55}$$

This point is also denoted by $\omega(\mathcal{A})$.

Proof: The property that the barycenters of the line-segments $(\mathsf{A}_-, \mathsf{A}_+)$ and $(\mathsf{B}_-, \mathsf{B}_+)$ coincide can be proved analogously to [49, Lemma 2]. Therefore, we can restrict to the orientational component. Without loss of generality we can assume a fixed system in a way that $\mathbf{A}_\mp = \mp(A_1, 0, 0)$ with $d \neq A_1 > 0$ and $\mathbf{B}_\mp = \mp(B_1, B_2, B_3)$ holds under the side-condition $B_1^2 + B_2^2 + B_3^2 = d^2$. Then, computation yields:

$$\begin{aligned} f_1(\mathcal{A}, \mathcal{B})^2 &= \tfrac{1}{3}(A_1^2 + 2A_1B_1 + B_1^2 + B_2^2 + B_3^2) = \tfrac{1}{3}(A_1^2 + 2A_1B_1 + d^2), \\ f_2(\mathcal{A}, \mathcal{B})^2 &= A_1^2 + 2A_1B_1 + B_1^2 + B_2^2 + B_3^2 = A_1^2 + 2A_1B_1 + d^2, \end{aligned} \tag{56}$$

which is in both cases minimal for $B_1 = -d$ (and maximal for $B_1 = d$). Therefore, we get $\mathbf{B}_\mp = \mp(d, 0, 0)$, which closes the proof. □

Note that if $\mathcal{A} \in \mathbb{R}^6 \setminus \Omega$ is located within the 3-dimensional space $\mathbf{A}_- = \mathbf{A}_+$ of $\mathbb{R}^6$, then the closest point on Ω is not uniquely defined. Every $\mathcal{B} \in \Omega$ with barycenter $\mathbf{A}_- = \mathbf{A}_+$ is a solution. Therefore, one has to make sure that c does not intersect this medial axis of Ω in step 1 of the algorithm.

Theorem 17. *The tangential hyperplane to Ω at point $(\mathbf{A}_-, \mathbf{A}_+) \in \Omega$ is given by*

$$\{(\mathbf{A}_- + \mathbf{V}_-, \mathbf{A}_+ + \mathbf{V}_+) \quad \textit{with} \quad \langle \mathbf{V}_+ - \mathbf{V}_-, \mathbf{A}_+ - \mathbf{A}_- \rangle = 0\}. \tag{57}$$

Proof: We consider points of a line l under a rigid body motion. It is well-known (e.g. [52, page 192]) that the projection of their velocity vectors orthogonally onto l is the same for all points on l. This so-called "Projection Theorem", which is illustrated in Figure 3 (right) already implies Theorem 17. □

Based on the last two theorems we implemented the outlined algorithm and computed the example illustrated in Figure 5.

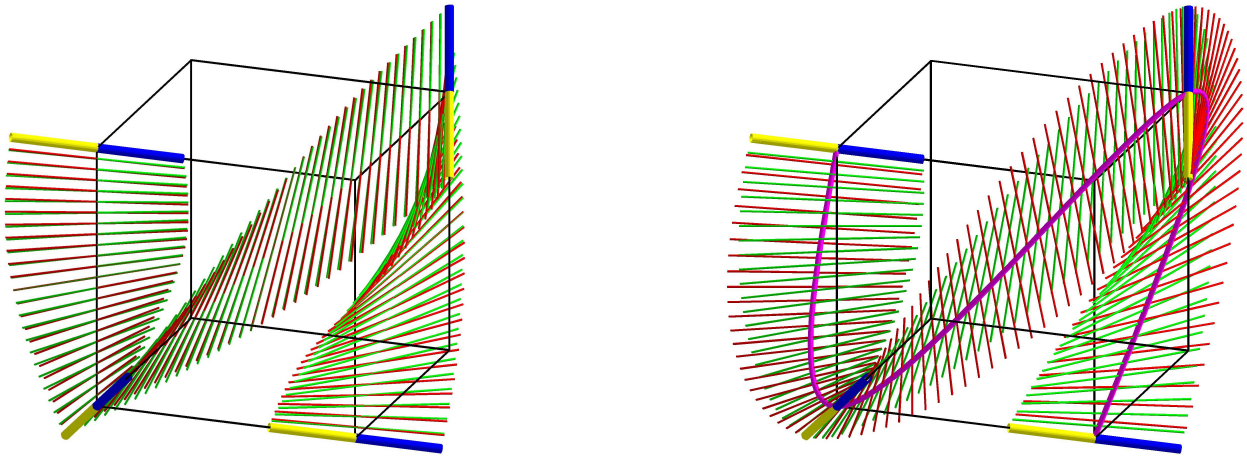

Figure 5: Four interpolate poses of an oriented line-segment are displayed in yellow/blue (indicating the orientation). Moreover, a cube is illustrated in order to improve the spatial sense of these poses. Left: The corresponding points of the four given poses in $\mathbb{R}^6$ are interpolated by three line-segments. Their projection onto Ω is illustrated in red. The geodesic motion is displayed in green. In both cases the barycenter of the line-segment moves along a straight line between two consecutive interpolate poses. Right: The minimizer of $E_b + 0.05E_g$ is illustrated in green and the interpolant with minimal bending energy is displayed in red. For the latter one the barycenter moves along a cubic C^2 spline (cf. [35, 50]), which is illustrated as magenta-colored curve.

5.2. Motion design based on De Casteljau's algorithm

In this section we explain how the famous algorithm of De Casteljau for Bézier curves can be adopted for the motion design of oriented line-elements. Given is a number k of control poses $(\mathsf{A}^i, \overrightarrow{\mathsf{a}}^i)$ for $i = 1, \dots, k$ of an oriented line-element $(\mathsf{A}, \overrightarrow{\mathsf{a}})$. Some possible strategies for applying the De Casteljau algorithm are as follows:

5.2.1. Projection algorithms

Assumed we have the point-model $\mathcal{P}$ located in the ambient space $\mathbb{R}^n$. Then, the control poses are points on $\mathcal{P}$, which are represented by the n-dimensional vector $\mathcal{A}^i$. Based on the control-polygon $\in \mathbb{R}^n$ we can compute the $k-1$ points $(\mathsf{A}^i_1, \overrightarrow{\mathsf{a}}^i_1)$ of the first step according to:

$$\mathcal{A}^i_1(t) := \mathcal{A}^i + t(\mathcal{A}^{i+1} - \mathcal{A}^i) \quad \text{for} \quad t \in [0,1] \quad \text{and} \quad i = 1, \dots, k-1. \tag{58}$$

This recursive procedure has to be done in total $k-1$ times, until we end up with the single point $\mathcal{A}^1_{k-1}(t)$, which traces the Bézier curve c in $\mathbb{R}^n$ by varying $t \in [0,1]$. Finally, c has to be projected back onto $\mathcal{P}$.

1. Clearly this can be done in the ambient space $\mathbb{R}^6$ of the point-model given in Theorem 15 and the back-projection is done by ω (see Figure 6 (left)).

2. Another possibility, which is illustrated in Figure 6 (right), is the following: Points of the ambient space $\mathbb{R}^7$ of the point-model given in Theorem 10 can be projected onto the quartic of Eq. (34) similarly to [53, Eq. (4)] by:

$$\iota : (\mathbf{a}, \widehat{\mathbf{a}}, a) \mapsto \left(\frac{\mathbf{a}}{\|\mathbf{a}\|}, \frac{\widehat{\mathbf{a}}}{\|\mathbf{a}\|} - \frac{\mathbf{a}\langle \mathbf{a}, \widehat{\mathbf{a}} \rangle}{\|\mathbf{a}\|^3}, \frac{a}{\|\mathbf{a}\|} \right). \tag{59}$$

   Remark 10. By skipping the 7th coordinate this mapping ι is a projection onto the dual unit-sphere $S^2_{\mathbb{D}}$ (Study model of oriented lines). The analog of this projection onto the dual unit-sphere $S^3_{\mathbb{D}}$ (cf. Eq. (7)) is implied by the fibers of the extended inverse kinematic map (cf. [54]). ◇

Both projection algorithms can be modified by projecting the points $\mathcal{A}^j_i(t)$, which are obtained after each iteration step, back onto $\mathcal{P}$. The resulting points are used for the next recursion.

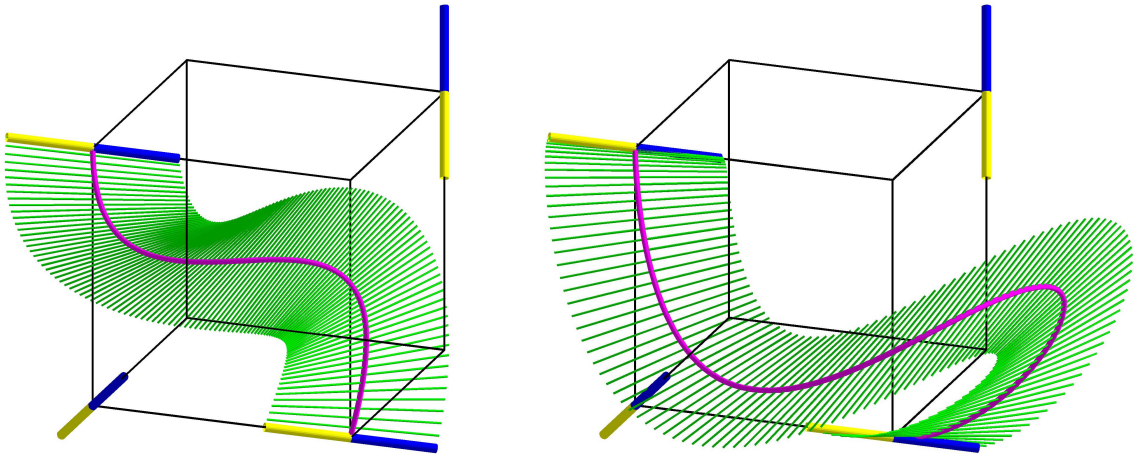

Figure 6: The same four poses of an oriented line-segment as in Figure 5 are now used as control poses. The motions resulting from both projection algorithms are displayed, where the trajectory of the oriented line-element's point (midpoint of the line-segment) is illustrated as curve. Left: Projection algorithm of item 1. Right: Projection algorithm of item 2.

5.2.2. Geodesic algorithms

The basic idea is to replace the straight line of the control polygon in the ambient space by their analog on the point-model $\mathcal{P}$, which are geodesics. In this way De Casteljau's algorithm always stays on $\mathcal{P}$ thus no back-projection onto $\mathcal{P}$ is required. For this purpose the geodesic motion of Section 5.1 is not practical (computationally inefficient), as it is the results of an optimization problem. Therefore, we are interested in geodesics between points of the point-model representing the oriented line-elements $(\mathsf{B}, \overrightarrow{\mathsf{b}})$ and $(\mathsf{A}, \overrightarrow{\mathsf{a}})$, those parametrization is known. Depending on the underlying metric (which itself is not of interest in this context), the following geodesics, which are illustrated in Figure 7 (upper left), can be deduced from the perspective of rigid-body motions:

1. According to Park [37] the geodesic motion can be composed by a translation with constant velocity along $\overrightarrow{\mathsf{BA}}$ and a simultaneous rotation with constant angular velocity bringing $\overrightarrow{\mathsf{b}}$ into $\overrightarrow{\mathsf{a}}$. As the rigid-body motion is incompletely defined (cf. Section 2.1) we choose the rotation in a way that the angle of rotation is minimal[6] ($\Rightarrow$ shortest geodesic). Therefore, the axis of rotation is orthogonal to $\overrightarrow{\mathsf{a}}$ and $\overrightarrow{\mathsf{b}}$.

2. Another approach taken by Ge and Ravani [55] is based on the representation of SE(3) by the dual unit-sphere $S^3_{\mathbb{D}}$. They showed that dual great circles (geodesics) on this sphere correspond to helical motions. Due to the incompleteness of our displacement we call again for a minimal angle of rotation (cf. footnote 6), which yields the screw motion given in Remark 3.

3. The last discussed geodesic is implied by the point-line displacement by Zhang and Ting (cf. Section 2.3), which is a composition of a screw motion about the common normal of $\overrightarrow{\mathsf{a}}$ and $\overrightarrow{\mathsf{b}}$ and a translation of B along the line $\overrightarrow{\mathsf{b}}$. If both is done simultaneously with constant speed we get the corresponding geodesic within the set of point-line displacements.

Remark 11. Under this motion the oriented line generates a so-called helicoid[7], which corresponds to the geodesic (dual great circles) on the Study model $S^2_{\mathbb{D}}$ of oriented lines (cf. [56]). Therefore, the geodesics of item 3 correspond to straight lines on the planar development of the cylinder over the corresponding dual great circle (cf. Remark 4). ◇

[6] With exception of the case that $\overrightarrow{\mathsf{a}}$ and $\overrightarrow{\mathsf{b}}$ are anti-parallel the geodesic motion is uniquely defined by this demand.

[7] This is the only ruled minimal surface. It is generated during a helical motion by a line intersecting the axis orthogonally.

The resulting three ”geodesic De Casteljau algorithms” are displayed in Figure 7 on the base of the same input data used for Figure 6. As these geodesic algorithms are computationally much more expensive than the projection algorithms, we recommend the latter ones for the task of interactive motion design. Under the assumption that the midpoint of the oriented line-segment is the point of the oriented line-element (cf. beginning of Section 3.2), the algorithm given in item 1 of Section 5.2.1 is very well suited, as its trajectory is the Bézier curve determined by the corresponding points of the control poses. This property has also the geodesic algorithm based on the geodesic motion of Park outlined in item 1 of Section 5.2.2 ($\Rightarrow$ the magenta curves of Figure 6 (left) and Figure 7 (upper right) are identical).

Finally, it should be noted that the procedures of Section 5.2 are not restricted to the algorithm of De Casteljau, but can easily be adapted for subdivision schemes like the Chaikin's algorithm or the interpolatory four-point scheme (cf. [57]).

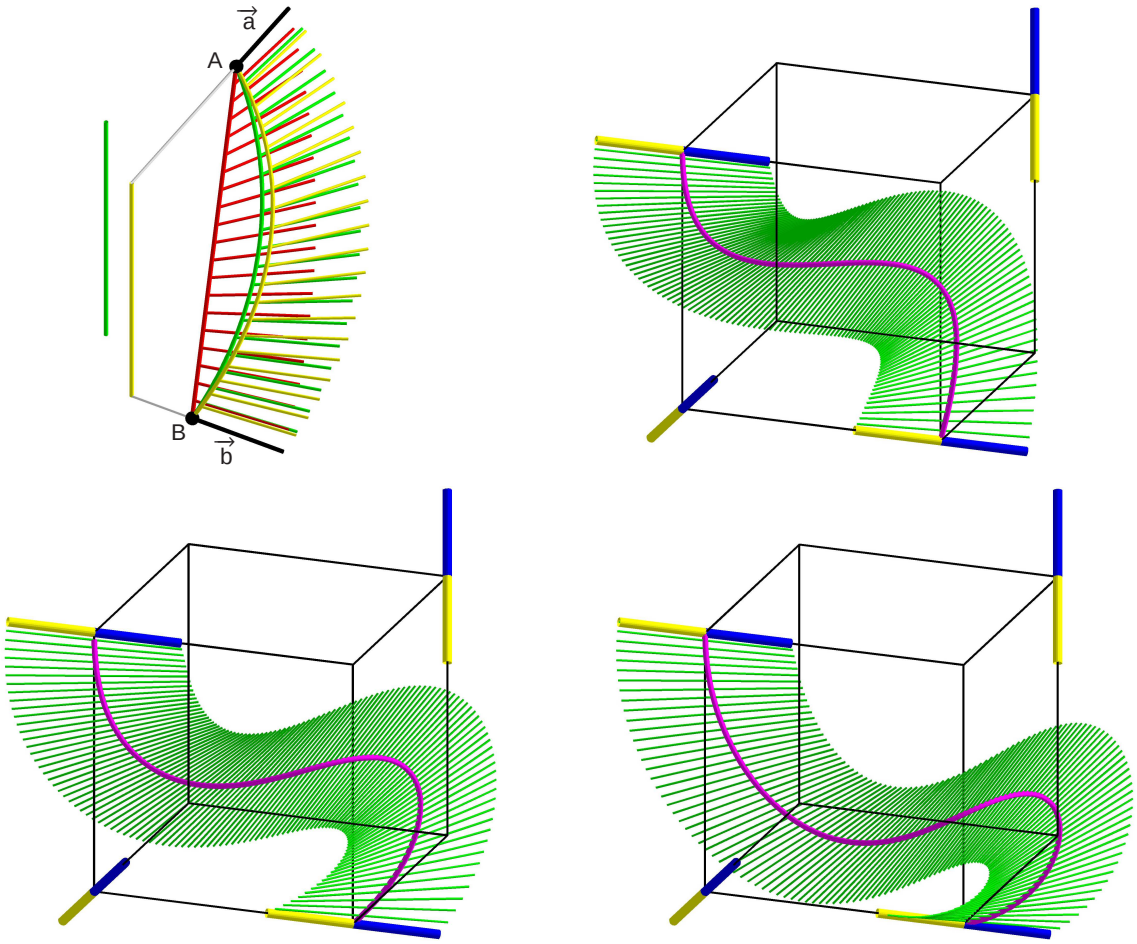

Figure 7: Upper left: The geodesic motions between two poses of an oriented line-element (black) are illustrated with respect to item 1 (red), item 2 (green) and item 3 (yellow), respectively. The trajectory of the corresponding point is displayed as curve. The yellow vertical line is the common normal of the given two poses of the oriented line-element and the green vertical line is the axis of the helical motion mentioned in item 2. The result of the geodesic algorithm based on the geodesic of item 1/2/3 is illustrated in the upper right/lower left/lower right corner.

6. Conclusion

Within this work it turned out that there is a large number of reasonable point-models for the set of oriented line-elements. Their degrees range between 2 and 20 and their codimensions between 1 and 10 (cf. Sections 2 and

3). The suitability of a point-model depends on the application having in mind; e.g. for the study of pentapods the point-model of Theorem 6 is very useful as shown in [28]. In Section 4 we showed that for path planning the point-model (hyperquadric Ω in $\mathbb{R}^6$) of Theorem 15 is in favor due to its compatibility with two geometric motivated metrics (the kinematic image space $\mathbb{R}^6$ is in both cases Euclidean). In addition, we pointed out in Section 5.1 that for these metric spaces well-known algorithms [49, 50] can be modified for (variational) motion design. Finally, we discussed in Section 5.2 different ways for adapting the famous algorithm of De Casteljau for the motion design of oriented line-elements.

Appendix

The ideal defining the variety described in Theorem 5 consists of six cubic equations

$$\begin{aligned}
g_{01}g_{24}g_{25} + 2g_{02}g_{25}g_{27} + g_{02}g_{03}g_{45} - g_{26}g_{27}g_{23} - g_{03}g_{46}g_{23} + g_{02}g_{47}g_{23} &= 0,\\
g_{01}g_{25}^2 + 2g_{03}g_{25}g_{27} + g_{03}^2g_{45} - g_{27}^2g_{23} + g_{01}g_{45}g_{23} &= 0,\\
2g_{02}g_{07}g_{27} - g_{01}g_{26}g_{27} - g_{02}g_{03}g_{67} - g_{06}g_{07}g_{23} &= 0,\\
2g_{03}g_{07}g_{27} + g_{01}g_{27}^2 - g_{03}^2g_{67} - g_{07}^2g_{23} - g_{01}g_{67}g_{23} &= 0,\\
g_{01}g_{24}g_{27} + 2g_{02}g_{27}^2 - g_{03}^2g_{46} + g_{02}g_{03}g_{47} - g_{06}g_{27}g_{23} &= 0,\\
g_{01}g_{25}g_{27} + 2g_{03}g_{27}^2 + g_{02}g_{03}g_{46} + g_{03}^2g_{47} - g_{07}g_{27}g_{23} + g_{01}g_{47}g_{23} &= 0,
\end{aligned}$$

36 quadratic equations

$$\begin{aligned}
g_{02}^2 + g_{03}^2 + g_{01}g_{23} &= 0, & g_{02}g_{04} - g_{01}g_{25} - g_{03}g_{27} &= 0, & g_{03}g_{04} + g_{01}g_{24} + g_{02}g_{27} &= 0,\\
g_{04}^2 + g_{27}^2 - g_{01}g_{45} &= 0, & g_{02}g_{06} + g_{03}g_{07} + g_{01}g_{27} &= 0, & g_{03}g_{06} - g_{02}g_{07} + g_{01}g_{26} &= 0,\\
g_{06}^2 + g_{07}^2 + g_{01}g_{67} &= 0, & g_{04}g_{06} - g_{07}g_{27} + g_{01}g_{47} &= 0, & g_{04}g_{07} + g_{06}g_{27} - g_{01}g_{46} &= 0,\\
g_{24}^2 + g_{25}^2 + g_{45}g_{23} &= 0, & g_{02}g_{24} + g_{03}g_{25} - g_{27}g_{23} &= 0, & g_{03}g_{24} - g_{02}g_{25} - g_{04}g_{23} &= 0,\\
g_{26}^2 + g_{27}^2 - g_{67}g_{23} &= 0, & g_{07}g_{24} + g_{26}g_{27} + g_{03}g_{46} &= 0, & g_{04}g_{24} + g_{25}g_{27} + g_{03}g_{45} &= 0,\\
g_{46}^2 + g_{47}^2 + g_{45}g_{67} &= 0, & g_{04}g_{25} - g_{24}g_{27} - g_{02}g_{45} &= 0, & g_{06}g_{25} - g_{26}g_{27} + g_{02}g_{47} &= 0,\\
g_{07}g_{25} - g_{27}^2 - g_{02}g_{46} &= 0, & g_{03}g_{26} + g_{02}g_{27} - g_{06}g_{23} &= 0, & g_{02}g_{26} - g_{03}g_{27} + g_{07}g_{23} &= 0,\\
g_{06}g_{24} - g_{27}^2 - g_{03}g_{47} &= 0, & g_{06}g_{26} + g_{07}g_{27} - g_{03}g_{67} &= 0, & g_{07}g_{26} - g_{06}g_{27} + g_{02}g_{67} &= 0,\\
g_{24}g_{26} - g_{25}g_{27} - g_{47}g_{23} &= 0, & g_{25}g_{26} + g_{24}g_{27} + g_{46}g_{23} &= 0, & g_{07}g_{45} - g_{04}g_{46} - g_{27}g_{47} &= 0,\\
g_{04}g_{26} - g_{27}^2 - g_{02}g_{46} - g_{03}g_{47} &= 0, & g_{27}g_{45} - g_{24}g_{46} - g_{25}g_{47} &= 0, & g_{06}g_{46} + g_{07}g_{47} + g_{27}g_{67} &= 0,\\
g_{04}g_{27} + g_{26}g_{27} + g_{03}g_{46} - g_{02}g_{47} &= 0, & g_{26}g_{46} + g_{27}g_{47} + g_{25}g_{67} &= 0, & g_{27}g_{46} - g_{26}g_{47} + g_{24}g_{67} &= 0,\\
g_{06}g_{45} + g_{04}g_{47} - g_{26}g_{47} + g_{24}g_{67} &= 0, & g_{26}g_{45} - g_{25}g_{46} + g_{24}g_{47} &= 0, & g_{07}g_{46} - g_{06}g_{47} + g_{04}g_{67} &= 0,
\end{aligned}$$

and the linear equation $g_{05} - g_{27} = 0$.

Acknowledgement. The research is supported by Grant No. P 24927-N25 of the Austrian Science Fund FWF.

References

[1] Selig, J.M.: Robot Kinematics and Flags. Applied Clifford algebra in cybernetics, robotics, image processing and engineering (E. Bayro-Corrochano, G. Sobczek eds.), pages 215–237, Birkhäuser, Boston (2001)
[2] Zhang, Y., Ting, K.-L.: On point-line geometry and displacement. Mechanism and Machine Theory **39** (10) 1033–1050 (2004)
[3] De Saussure, R.: Sur le Mouvement d'une droite qui possède trois degrés de liberté. Comptes Rendus **133** 1283–1285 (1902)
[4] De Saussure, R.: Géométrie des Feuillets. Archives des Sciences Physiques et Naturelles de Genéve **21** 134–155 (1906)
[5] Odehnal, B.: Flags in Euclidean three-space. Mathematica Pannonica **17** (1) 29–48 (2006)
[6] Odehnal, B.: The geometry of flags. Proceedings of Algebraic Geometry and Geometric Modeling, pages 101–106 (2006)
[7] Study, E.: Geometrie der Dynamen. B.G. Teubner, Leipzig (1903)
[8] Blaschke, W.: Euklidische Kinematik und nichteuklidische Geometrie. Zeitschrift für Mathematik und Physik **60** 61–91 and 203–204 (1911)

[9] Grünwald, J.: Ein Abbildungsprinzip, welches die ebene Geometrie und Kinematik mit der räumlichen Geometrie verknüpft. Sitz.-Ber. der math.-nat. Klasse der kaiserlichen Akademie der Wissenschaften Wien **120** 677–741 (1911)
[10] Röschel, O.: Rational motion design – a survey. Computer-Aided Design **30** (3) 169–178 (1998)
[11] Jüttler, B., Wagner, M.: Kinematics and Animation. Handbook of Computer Aided Geometric Design (G. Farin et al eds.) pages 723–748, North Holland (2001)
[12] Gfrerrer, A.: Study's kinematic mapping – a tool for motion design. Advances in Robot Kinematics (J. Lenarcic, M.M. Stanisic eds.), pages 7–16, Kluwer (2000)
[13] Schröcker, H.-P., Jüttler, B.: Motion Interpolation with Bennett Biarcs. Computational Kinematics (A. Kecskemethy, A. Müller eds.), pages 101–108, Springer (2009)
[14] Nawratil, G.: Quaternionic approach to equiform kinematics and line-elements of Euclidean 4-space and 3-space. Computer Aided Geometric Design **47** 150–162 (2016)
[15] Selig, J.M.: Geometric Fundamentals of Robotics. Springer, 2nd Edition (2005)
[16] Pottmann, H., Wallner, J.: Computational Line Geometry. Springer (2001)
[17] Bottema, O.: On a Set of Displacements in Space. ASME Journal of Engineering for Industry **95** 451–454 (1973)
[18] Tsai, L.-W., Roth, B.: Incompletely Specified Displacements: Geometry and Spatial Linkage Synthesis. ASME Journal of Engineering for Industry **95** 603–611 (1973)
[19] Sticher, F.: On the finite screw axis cylindroid. Mechanism and Machine Theory **24** (3) 143–155 (1989)
[20] Parkin, I.A.: A third conformation with the screw systems: finite twist displacements of a directed line and point. Mechanism and Machine Theory **27** (2) 177–188 (1992)
[21] Huang, C., Roth, B.: Analytic expressions for the finite screw systems. Mechanism and Machine Theory **29** (2) 207–222 (1994)
[22] Hunt, K.H., Parkin, I.A.: Finite displacements of points, planes, and lines via screw theory. Mechanism and Machine Theory **30** (2) 177–192 (1995)
[23] Ramahi, A., Tokad, Y.: On the Finite Screw Cylindroid Represented as a 2-system of Screws. Meccanica **33** 111–125 (1998)
[24] Zhang, Y., Ting, K.-L.: On the basis screws and screw systems of point-line and line displacement. ASME Journal of Mechanical Design **126** 56–62 (2004)
[25] Schoenflies, A.: Geometrie der Bewegung in synthetischer Darstellung. G. Teubner (1886)
[26] Shafarevich, I.R.: Algebraic Geometry. Springer (1988)
[27] Zhang, X.M., Zhu, L.M., Ding, H., Xiong, Y.L.: Kinematic generation of ruled surface based on rational motion of point-line. Science China Technological Sciences **55** (1) 62–71 (2012)
[28] Nawratil, G., Schicho, J.: Self-motions of pentapods with linear platform. Robotica (in press) [arXiv:1407.6126]
[29] Odehnal, B., Pottmann, H., Wallner, J.: Equiform kinematics and the geometry of line elements. Beiträge zur Algebra und Geometrie **47** (2) 567–582 (2006)
[30] Klawitter, D.: Clifford Algebras. Geometric Modelling and Chain Geometries with Application in Kinematics. Springer Spektrum, Wiesbaden (2015)
[31] Odehnal, B.: Die Linienelemente des P^3. Österreich. Akad. Wiss. Math.-Naturw. Kl. S.-B. II **215** 155–171 (2006)
[32] Combebiac, G.: Calcul des triquaternions. Bulletin de la Societe Mathematique de France **27** 180–194 (1899)
[33] Ravani, B., Wang, J.W.: Computer Aided Geometric Design of Line Constructs. Journal of Mechanical Design **113** 363–371 (1991)
[34] Ge, Q.J., Ravani, B.: On representation and interpolation of line-segments for computer aided geometric design. Advances in Design Automation **69** (1) 191–198 (1994)
[35] Chen, H.Y., Pottmann, H.: Approximation by ruled surfaces. Journal of Computational and Applied Mathematics **102** 143–156 (1999)
[36] Zhang, Y., Ting, K.-L.: Point-line Distance Under Riemannian Metrics. ASME Journal of Mechanical Design **130** 092304 (2008)
[37] Park, F.C.: Distance Metrics on the Rigid-Body Motions with Applications to Mechanism Design. ASME Journal of Mechanical Design **117** 48–54 (1995)
[38] Kazerounian, K., Rastegar, J.: Object Norms: A Class of Coordinate and Metric Independent Norms for Displacements. Flexible Mechanisms, Dynamics and Analysis (G.L. Kinzel ed.), pages 271–275, ASME (1992)
[39] Chen, L., Xu, K., Tang, K.: Collision-free tool orientation optimization in five-axis machining of bladed disk. Journal of Computational Design and Engineering **2** (4) 197–205 (2015)
[40] Pottmann, H., Hofer, M., Ravani, B.: Variational motion design. On Advances in Robot Kinematics (J. Lenarcic, C. Galletti eds.) pages 361-370, Kluwer (2004)
[41] Gfrerrer, A.: On the Construction of Rational Curves on Hyperquadrics. Habilitation thesis, Graz University of Technology (2001)
[42] Wang, W.; Joe, B.: Interpolation on quadric surfaces with rational quadratic spline curves. Computer Aided Geometric Design **14** (3) 207–230 (1997)
[43] Koch, J.: Method of directing the movement of a tool as part of a process to remove material from a block of material. Patent US 6632053 (2001)
[44] Langeron, J.M., Duc, E., Lartigue, C., Bourdet, P.: A new format for 5-axis tool path computation, using Bspline curves. Computer-Aided Design **36** (12) 1219–1229 (2004)
[45] Fleisig, R.V., Spence, A.D.: A constant feed and reduced angular acceleration interpolation algorithm for multi-axis machining. Computer-Aided Design **33** (1) 1–15 (2001)
[46] Dietz, R., Hoschek, J., Jüttler, B.: An algebraic approach to curves and surfaces on the sphere and on other quadrics. Computer Aided Geometric Design **10** (3-4) 211–229 (1993)
[47] Popiel, T., Noakes, L.: C^2 spherical Bézier splines. Computer Aided Geometric Design **23** (3) 261–275 (2006)
[48] Wu, Y., Müller, A., Carricato, M.: The 2D Orientation Interpolation Problem: A Symmetric Space Approach. Advances in Robot Kinematics (J. Lenarcic, J.-P. Merlet eds.), pages 297–305, HAL (2016)
[49] Hofer, M.: Variational Motion Design in the Presence of Obstacles. PhD-Thesis, Vienna University of Technology (2004)
[50] Hofer, M., Pottmann, H.: Energy-Minimizing Splines in Manifolds. ACM Transactions on Graphics **23** (3) 284-293 (2004)

[51] Flöry, S., Hofer, M.: Constrained curve fitting on manifolds. Computer-Aided Design **40** (1) 25–34 (2008)
[52] Bottema, O., Roth, B.: Theoretical Kinematics. North-Holland Publishing Company (1979)
[53] Odehnal, B.: Subdivision Algorithms for Ruled Surfaces. Journal for Geometry and Graphics **12** (1) 1–18 (2008)
[54] Pfurner, M., Schröcker, H.-P., Husty, M.: Path Planning in Kinematic Image Space Without the Study Condition. Advances in Robot Kinematics (J. Lenarcic, J.-P. Merlet eds.), pages 290–297, HAL (2016)
[55] Ge, Q.J., Ravani, B.: Geometric Construction of Bézier Motions. Journal of Mechanical Design **116** (3) 749–755 (1994)
[56] Sprott, K., Ravani, B.: Kinematic generation of ruled surfaces. Advances in Computational Mathematics **17** 115–133 (2002)
[57] Wallner, J., Pottmann, H.: Instrinsic Subdivision with Smooth Limits for Graphics and Animation. ACM Transactions on Graphics **25** (2) 356–374 (2006)